

ChemComm

Accepted Manuscript



This is an *Accepted Manuscript*, which has been through the Royal Society of Chemistry peer review process and has been accepted for publication.

Accepted Manuscripts are published online shortly after acceptance, before technical editing, formatting and proof reading. Using this free service, authors can make their results available to the community, in citable form, before we publish the edited article. We will replace this *Accepted Manuscript* with the edited and formatted *Advance Article* as soon as it is available.

You can find more information about *Accepted Manuscripts* in the [Information for Authors](#).

Please note that technical editing may introduce minor changes to the text and/or graphics, which may alter content. The journal's standard [Terms & Conditions](#) and the [Ethical guidelines](#) still apply. In no event shall the Royal Society of Chemistry be held responsible for any errors or omissions in this *Accepted Manuscript* or any consequences arising from the use of any information it contains.

Cite this: DOI: 10.1039/coxx00000x

www.rsc.org/xxxxxx

ARTICLE TYPE

Single-Nanoparticle NO₂ Gas Sensor Using Active Molecular Plasmonics

Lichan Chen, Bo Wu, Longhua Guo, Ruiwen Tey, Youju Huang, Dong-Hwan Kim

Received (in XXX, XXX) Xth XXXXXXXXX 20XX, Accepted Xth XXXXXXXXX 20XX

DOI: 10.1039/b000000x

5 A single-nanoparticle plasmonic sensor for the sensitive detection of gas molecule (NO₂) has been constructed. Taking advantage of active molecular plasmonics, the analyte selectively trigger a measurable spectral shift of ferrocene-modified single gold nanorods.

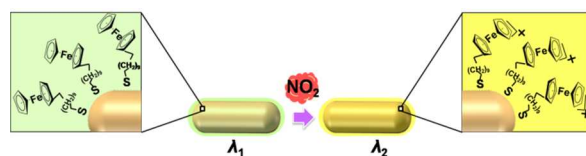
10 Plasmonic sensing that utilizes spectral response of metal nanoparticles to the refractive index (RI) of surrounding medium has been explored for various areas of applications, including disease diagnostics,¹ food safety,² and biomedical assays.³ To date, these applications have been primarily focused on biological detection^{1,4-6} because the spectral response of metal nanoparticles requires a large change in surrounding RI; which can be readily obtained from the binding event of bulky biomolecules. On the contrary, a limited number of studies have been conducted on small molecules.⁷ Particularly, gas sensing based on localized surface plasmon resonance (LSPR) has been known to be challenging because gas molecules generally exhibit low adsorption efficiency to metal surface and the adsorption of gas molecules on plasmonic particles induces minute RI changes.

To improve sensing capabilities of LSPR-based gas sensors several strategies were previously explored. Karakouz et al. developed plasmonic nanoparticles modified with a layer of polymer to mediate preferential adsorption of gaseous analytes.^{8,9} This scheme relies on the association of molecules arising from similar polarity; thus limited with poor selectivity. Alivisatos's group constructed a resonance gold (Au) antenna-enhanced hydrogen sensor by taking advantage of the high adsorption ability of palladium (Pd) towards hydrogen.¹⁰ This sensor showed high sensitivity of hydrogen detection but the fabrication of Au-Pd nanostructures required sophisticated manufacturing process. Van Duyne's group developed a high resolution LSPR spectroscopy for the measurement of a small RI change of gas molecules (i.e., RI unit of $\sim 10^{-4}$).¹¹ After that, they managed to amplify the sensing signal over an order of magnitude by pre-concentrating gas molecules in a porous metal-organic framework grown on the surface of nanoparticles.⁷ However, this approach is limited to pure gas detection because of lack of a capturing probe. Therefore, selective and sensitive detection of gas molecules in complex media still faces large challenges.

Here, we present a new plasmonic gas sensing strategy by employing active molecular plasmonics. Active molecular plasmonic system utilizes metal/molecule complexes; the LSPR peak location of metal nanostructures shifts via the interactions between molecular resonance and the LSPR of the metal

nanostructures,¹²⁻¹⁶ and the resulting LSPR shift is strongly dependent on the spectral overlap between the two resonances.^{12,17} Recently, we discovered that NO₂ can trigger the chemical oxidation of ferrocene because of strong electron-withdrawing ability of NO₂ (Fig. 1A). Ferrocenium, the oxidative product of ferrocene, shows much difference in absorption frequency from ferrocene because of their unique electronic structures (Scheme 1). Coupling between the molecular resonance of ferrocenium and the LSPR of Au nanostructure can be mediated by switching the electronic resonance between ferrocene and ferrocenium. Therefore, we expect that, when the molecular resonance of ferrocenium overlaps with plasmonic peak of Au nanoparticles, an Au nanoparticle conjugated with ferrocene provides a significant spectral shift, serving as a selective probe for NO₂.

Based on the speculation, we performed the single-nanoparticle LSPR gas detection in a newly designed microfluidic chip. Our nanoplasmonic probe provides high sensitivity by i) amplifying sensing signal via active molecular plasmonics, ii) performing the detection at the single-particle level. Single-entity measurement not only eliminates the statistical and average characteristics inherent to ensemble measurement; hence providing better signal/noise resolution and higher sensitivity, but also offers a unique tool for probing individual behavior and process to understand the influence of LSPR wavelength of nanostructure on the sensing performance. In addition, the proposed LSPR gas sensor offers high specificity through the selective oxidation of ferrocene attached on gold nanoparticles.



Scheme 1 Schematic illustration of the NO₂ detection using active molecular plasmonic.

To realize the single-nanoparticle-based LSPR gas sensor, a double-layer glass/PDMS hybrid microfluidic chip that provides high-resolution images and spectra of single nanoparticles under dark-field microscopy system¹⁸ was fabricated (Fig. 1B). For the microfluidic chip design, PDMS was selected due to its well-known features, including optical clarity, high permeability to gas molecules, and accessible micro-fabrication techniques.^{19,20} The thickness of the microfluidic chip should be accurately controlled, because the typical maximum thickness of the sample slide for a

set of $100 \times$ oil-immersion objective lens and condenser is fixed, (e.g., ~ 1.3 mm in our dark field system).²⁰ The microfluidic chip was constructed with two layers: the upper air channel for flow rate controllable ventilation, and the bottom fluidic channel that was sealed to a thin glass substrate where metal nanoparticle/molecule complex are located. Diffusion of NO_2 gas between the two layers readily occurs across a thin PDMS membrane (5 μm) due to the high permeability of PDMS to NO_2 gas.²¹ Compared with its predecessor that used fused glass μ -channel,²² the glass/PDMS hybrid microfluidic chip is easy to fabricate and manufacturing process in a high temperature is not required. The detail fabrication procedure and the image of an actual device are shown in supporting information.

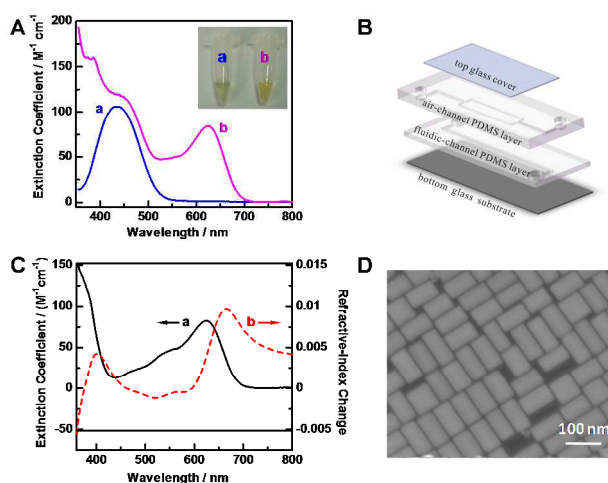


Fig. 1 A) The absorption spectra of 5 mM ferrocene in acetonitrile solution before (curve a) and after (curve b) oxidation by NO_2 . Inset: photos of ferrocene in acetonitrile solution before (a) and after (b) oxidation. The ferrocene solution showed an absorption peak at 435 nm, whereas the ferrocenium obtained from the oxidation of ferrocene by NO_2 displayed a peak at 625 nm. B) Schematic illustration of the microfluidic device. C) The oxidation-induced refractive-index change (curve b) of ferrocene was derived from the differential absorption spectrum (curve a) by using the Kramers-Kronig equation. D) Typical SEM image of AuNRs used in this work.

When resonant molecules interact with noble metal nanoparticles, the induced LSPR peak shift are sensitive to the wavelengths of each contributors on the active molecular plasmonics.¹⁷ Accordingly, to obtain the maximal LSPR shift in the event of change of ferrocene to ferrocenium, it is critical to optimize the LSPR peak location of the ferrocene-modified gold nanoparticle. It has been proved that in most cases, the dependence of the induced peak shift on the wavelength of gold nanoparticle modified with resonant molecules tracks with the wavelength dependence of the resonance molecule's refractive index.¹⁷ The wavelength-dependent refractive index of the resonant molecules can be estimated from Kramers-Kronig equation,^{17, 23} which essentially relates the molecular absorption spectrum to the refractive index. In line with this, the maximum LSPR shift can be achieved by locating the peak of resonant molecules-modified plasmonic nanoparticle at the wavelength where the resonant molecule shows the maximal refractive index.

Herein, on the basis of the UV-vis absorption spectra of ferrocene and ferrocenium in acetonitrile (Fig. 1A), we firstly determined the change in refractive index (Δn) of ferrocene and ferrocenium by using the Kramers-Kronig transformation

$$\Delta n(\omega') = \frac{c}{\pi} \int_0^{\infty} \frac{\Delta\alpha(\omega)}{\omega^2 - (\omega')^2} d\omega \quad (1)$$

Where c is the speed of light, ω is the angular frequency ($\omega = 2\pi c/\lambda$, λ is the wavelength of light), $\Delta\alpha$ is the difference in extinction coefficient between ferrocene and ferrocenium, as shown in Fig. 1C curve a ($\Delta\alpha = 2.303 A(\lambda)/T$, where $A(\lambda)$ is the molecular absorbance at a given wavelength and T is the effective molecular thickness). The refractive index difference between ferrocene and ferrocenium as a function of wavelength (Fig. 1C, curve b) indicates that the refractive index change is maximal at the wavelength of 665 nm.

In our experiment, a gold nanorod conjugated with ferrocene (AuNR-Fc) was adapted to construct a nanoplasmonic probe for sensing NO_2 . The use of AuNR is because the longitudinal plasmon resonance wavelength of AuNR could be precisely adjusted by the length-to-diameter aspect ratio, and they show reduced plasmon damping compared to Au nanosphere.²⁴ AuNRs with an ensemble longitudinal LSPR wavelength of 660 nm (measured by UV-vis spectrometer, Fig. S1, curve b) were synthesized by using a tip overgrowth method.²⁵⁻²⁷ As shown in Fig. 1D, the obtained AuNRs were 96.7 ± 5.6 nm in length and 52.1 ± 3.6 nm in diameter ($n = 150$). The AuNR-Fc probe was fabricated by the immobilization of AuNRs on glass substrate in the fluidic-channel via electrostatic interaction followed by self-assembly (SAM) of 11-(Ferrocenyl) undecanethiol (FcC_{11}SH) on the surface of AuNR through Au-S chemistry. The scattering images and spectra of individual AuNR-Fc probes were acquired using a dark-field microscopy with a true color imaging CCD and a spectrometer.¹⁸ The inset image of selected area and the spectra of selected AuNR-Fc probe in Fig. 2A obtained on the custom-designed microfluidic device indicate the feasibility of the PDMS-microchannel for dark-field microscopy imaging and spectrum acquiring. Aggregates and impurities, as judged by color and scattering profile, were ruled out in the following analyses as previously reported.^{18, 28} During the formation of

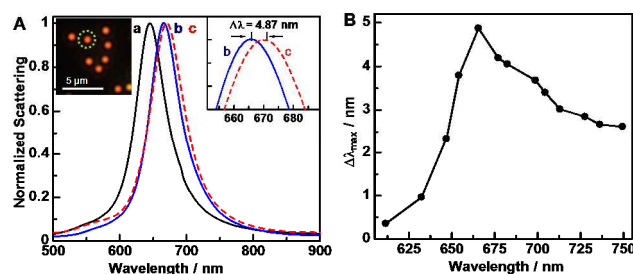


Fig. 2 A) Steady-state LSPR spectra recorded from (a) Au nanorod, (b) ferrocene-modified Au nanorod (AuNR-Fc) in acetonitrile with an initial peak wavelength of 665.28 nm, (c) (b) upon injection of 100 ppm NO_2 gas. The inset curve shows the peak wavelength shift of 4.87 nm upon the oxidation of ferrocene induced by NO_2 . The inset image shows the dark field image of the selected AuNR-Fc (i.e. in the green circle). B) Plot of the experimental LSPR shift vs spectral position of the AuNR-Fc probes upon injection of 100 ppm NO_2 .

FcC₁₁SH SAM, the scattering spectra of individual probe were monitored until the peak location remains unchanged. After the deposition of SAM, the spectrum wavelength of the selected probe red-shifted from 644.75 nm (Fig. 2A, curve a) to 665.28 nm (Fig. 2A, curve b), indicating the increase in the refractive index of surroundings.²⁹

To verify the feasibility of the active molecular plasmonic gas sensor for the detection of NO₂, 100 ppm NO₂ gas was applied to AuNR-Fc mounted in the microfluidic device. As shown in Fig. 2A curve c, the scattering peak red-shifted by 4.87 nm from 665.28 to 670.15 nm after NO₂ injection. To confirm the unique correlation between NO₂-triggered oxidation of ferrocene and corresponding LSPR peak shift, three control experiments were separately carried out. In the first control experiment performed using a bare AuNR without ferrocene, no measurable peak shift was obtained even when high concentration of NO₂ was applied (up to 2000 ppm) (see Fig. S3A). In the second control experiment a AuNR modified with a nonresonant molecule, 6-mercaptohexanol, was employed. Similar to the first control experiment, almost no peak shift was observed when 2000 ppm NO₂ was applied (see Fig. S3B). In the third control experiment performed using AuNR-Fc, no peak shift was observed upon the injection of pure N₂ gas (see Fig. S3C). These results indicated that the spectral shift was induced solely by the resonance coupling between the oxidized ferrocene and AuNR. In addition to the refractive index change resulted from the oxidation of ferrocene to ferrocenium as mentioned above, other probable factors that contribute to the spectral shift are described in the supporting information.

Next, the dependence of the spectral shift on the wavelength of the AuNR-Fc probe was investigated by testing the AuNR-Fc probes with initial peak wavelengths ranging from 610 to 750 nm. Fig. 2B shows that the maximum spectral shift is obtained at the wavelength of around 665 nm, and suggests that the dependence of the peak shift on wavelength tracks with the wavelength dependence of the resonance molecule's refractive index as determined by the Kramers-Kronig equation (Fig. 1C, curve b). The result indicates that the refractive index change resulted from oxidation of ferrocene to ferrocenium and the molecular-plasmonic resonance coupling play a leading role for the spectral shift. Therefore, NO₂ can act as an efficient trigger to activate molecular plasmonics by mediating the interactions between molecular resonance of ferrocene/ferrocenium system and plasmon resonance of AuNR.

Having established that NO₂ can activate a shift of the scattering wavelength of AuNR-Fc probe, we investigated the sensing performance of the probe in detail. To evaluate the sensitivity, different concentrations of NO₂ ranged from 0.1 to 4000 ppm were tested. Fig. 3 shows the dose-response curve obtained from the average scattering wavelength shifts of 30 individual AuNR-Fc with peak wavelength around 665 nm. The wavelength shift is dependent on the concentration of NO₂ gas. Initially, the shift increased with increasing concentrations of NO₂ gas in the range of 0.1-2000 ppm, reached a maximum at 2000 ppm, and then decreased with further increase of NO₂ gas concentration. Below 2000 ppm, the oxidation of ferrocene by NO₂ played a dominant role, which resulted in increasing ferrocenium concentration on the surface of AuNR, thus

enhancing the induced plasmon shift. To further confirm the effect of NO₂ concentration on the ferrocene oxidation, a control experiment was carried out by using an electrochemical method (see SI). However, above 2000 ppm, the decreases in spectral shift were observed probably due to the ability of NO₂ to oxidize thiols; NO₂ reduces the thiol's affinity to bind to gold and severely affects the stability of the ferrocenium layer.³⁰ The limit of detection of NO₂ was calculated to be 100 ppb determined by an average wavelength shift of 0.65 nm (S/N=3). Furthermore, the relative standard deviations (RSDs) of the steady-state responses of the present nanoplasmonic gas sensor were less than 10%, which is comparable to the reusable single-nanoparticle plasmonic sensor.³¹ The excellent reproducibility may be attributed to the facts that the plasmon energy, instead of the morphological feature of AuNRs, and local electric field enhancement played the major role in the coupling between AuNR and ferrocenium.³²

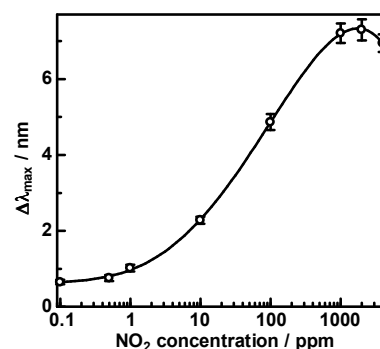


Fig. 3 Dose-response curve for NO₂ detection. Each data point was averaged from LSPR shifts of 30 AuNR-Fc probes and the error bars represent standard deviations.

The selectivity of this system was explored by testing the response of the sensor to other possibly co-existing gases, including SO₂, NH₃ and H₂S at the concentration of 1000 ppm, as well as CO₂ at 10000 ppm. Fig. 4 summarizes the sensing response of the developed plasmonic sensor to other gases. Our nanoplasmonic probe generates negligible change in the scattering wavelength when exposed to other gases at high concentrations, suggesting good selectivity in sensing NO₂. The great selectivity results from the fact that all of these interfering gases cannot oxidize ferrocene to ferrocenium, which was confirmed by the experiment that treatments of the interfering

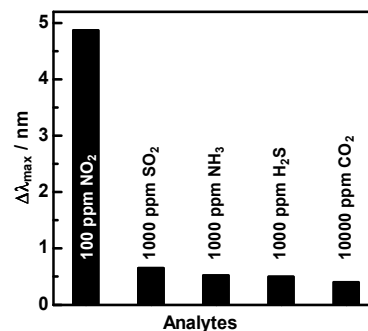


Fig. 4 Plasmonic responses of the as-developed plasmonic sensor to various gases.

gases with ferrocene in acetonitrile give rise to no change in adsorption spectra (data not shown). Nevertheless, we note that AuNR-Fc may exhibit interferences with other oxidizing gases (e.g., Cl₂ and ozone) because the proposed sensor was developed based on the electron-withdrawing capability of NO₂.

In summary, we developed an active-molecular-plasmonics-based sensing platform to selectively and sensitively detect NO₂, an air pollutant that induces acidic rain and causes increased incidence of acute respiratory illness.^{33, 34} A double layer microfluidic device was fabricated to promote the performance of the single-nanoparticle LSPR gas sensor. The Kramers-Kronig analysis was employed to optimize the wavelength of AuNR-Fc probe for achieving the maximal spectral shift, which was consistent with the experimental data. High detection sensitivity of the proposed sensor is attributed to the signal amplification sensing strategy via active-molecular-plasmonics and the inherent advantage of single-nanoparticle-based sensing. In addition, benefited from the fact that the co-existing gaseous substances in atmosphere cannot oxidize ferrocene, the developed sensing system exhibited excellent selectivity.

We acknowledge financial support from the Ministry of Education (MOE2012-T2-1-058) of Singapore.

Notes and references

^aSchool of Chemical and Biomedical Engineering, Nanyang Technological University, 70 Nanyang Drive, Singapore 637457, Singapore. Fax: +65 6791 1761; Tel: +65 6790 4111; E-mail: dhkim@ntu.edu.sg

† Electronic Supplementary Information (ESI) available: [Experimental section, and Figures S1-S4.]. See DOI: 10.1039/b000000x/

- A. J. Haes, L. Chang, W. L. Klein and R. P. Van Duyne, *J. Am. Chem. Soc.*, 2005, **127**, 2264-2271.
- L. Guo, Y. Xu, A. R. Ferhan, G. Chen and D.-H. Kim, *J. Am. Chem. Soc.*, 2013, **135**, 12338-12345.
- K. M. Mayer and J. H. Hafner, *Chem. Rev.*, 2011, **111**, 3828-3857.
- A. J. Haes and R. P. Van Duyne, *J. Am. Chem. Soc.*, 2002, **124**, 10596-10604.
- C. Yu and J. Irudayaraj, *Anal. Chem.*, 2006, **79**, 572-579.
- J. N. Anker, W. P. Hall, O. Lyandres, N. C. Shah, J. Zhao and R. P. Van Duyne, *Nat. Mater.*, 2008, **7**, 442-453.
- L. E. Kreno, J. T. Hupp and R. P. Van Duyne, *Anal. Chem.*, 2010, **82**, 8042-8046.
- T. Karakouz, A. Vaskevich and I. Rubinstein, *J. Phys. Chem. B*, 2008, **112**, 14530-14538.
- Y.-Q. Chen and C.-J. Lu, *Sens. Actuators B Chem*, 2009, **135**, 492-498.
- N. Liu, M. L. Tang, M. Hentschel, H. Giessen and A. P. Alivisatos, *Nat. Mater.*, 2011, **10**, 631-636.
- J. M. Bingham, J. N. Anker, L. E. Kreno and R. P. Van Duyne, *J. Am. Chem. Soc.*, 2010, **132**, 17358-17359.
- Y. B. Zheng, Y.-W. Yang, L. Jensen, L. Fang, B. K. Juluri, A. H. Flood, P. S. Weiss, J. F. Stoddart and T. J. Huang, *Nano Lett.*, 2009, **9**, 819-825.
- J. Dintinger, S. Klein and T. W. Ebbesen, *Advanced Materials*, 2006, **18**, 1267-1270.
- G. A. Wurtz, P. R. Evans, W. Hendren, R. Atkinson, W. Dickson, R. J. Pollard, A. V. Zayats, W. Harrison and C. Bower, *Nano Lett.*, 2007, **7**, 1297-1303.
- N. T. Fofang, T.-H. Park, O. Neumann, N. A. Mirin, P. Nordlander and N. J. Halas, *Nano Lett.*, 2008, **8**, 3481-3487.
- J. Zhao, A. Das, X. Zhang, G. C. Schatz, S. G. Sligar and R. P. Van Duyne, *J. Am. Chem. Soc.*, 2006, **128**, 11004-11005.
- A. J. Haes, S. Zou, J. Zhao, G. C. Schatz and R. P. Van Duyne, *J. Am. Chem. Soc.*, 2006, **128**, 10905-10914.
- L. Guo, A. R. Ferhan, K. Lee and D.-H. Kim, *Anal. Chem.*, 2011, **83**, 2605-2612.
- E. A. Lemke, Y. Gambin, V. Vandelinder, E. M. Brustad, H.-W. Liu, P. G. Schultz, A. Groisman and A. A. Deniz, *J. Am. Chem. Soc.*, 2009, **131**, 13610-13612.
- Y. Luo, W. Sun, C. Liu, G. Wang and N. Fang, *Anal. Chem.*, 2011, **83**, 5073-5077.
- S. Mertes and A. Wahner, *J. Phys. Chem.*, 1995, **99**, 14000-14006.
- L. Guo, Y. Huang, Y. Kikutani, Y. Tanaka, T. Kitamori and D.-H. Kim, *Lab on a Chip*, 2011, **11**, 3299-3304.
- R. d. L. Kronig and H. A. Kramers, *Z. Phys.*, 1928, **48**, 174-179.
- C. Sönnichsen, T. Franzl, T. Wilk, G. von Plessen, J. Feldmann, O. Wilson and P. Mulvaney, *Phys. Rev. Lett.*, 2002, **88**, 077402.
- B. Nikoobakht and M. A. El-Sayed, *Chem. Mater.*, 2003, **15**, 1957-1962.
- K. Sohn, F. Kim, K. C. Pradel, J. Wu, Y. Peng, F. Zhou and J. Huang, *ACS Nano*, 2009, **3**, 2191-2198.
- Y. Huang, A. R. Ferhan and D.-H. Kim, *Nanoscale*, 2013, **5**, 7772-7775.
- A. M. Funston, C. Novo, T. J. Davis and P. Mulvaney, *Nano Lett.*, 2009, **9**, 1651-1658.
- A. D. McFarland and R. P. Van Duyne, *Nano Lett.*, 2003, **3**, 1057-1062.
- M. J. Coutts, M. B. Cortie, M. J. Ford and A. M. McDonagh, *J. Phys. Chem. C*, 2009, **113**, 1325-1328.
- L. Guo and D.-H. Kim, *Chem. Commun.*, 2011, **47**, 7125-7127.
- W. Ni, H. Chen, J. Su, Z. Sun, J. Wang and H. Wu, *J. Am. Chem. Soc.*, 2010, **132**, 4806-4814.
- P. L. Keblanian, S. C. Herndon and A. Freedman, *Anal. Chem.*, 2004, **77**, 724-728.
- D. Zhang, Z. Liu, C. Li, T. Tang, X. Liu, S. Han, B. Lei and C. Zhou, *Nano Lett.*, 2004, **4**, 1919-1924.